Soft Matter

PAPER

Cite this: *Soft Matter*, 2019, **15**, 5227

Periodic buckling and grain boundary slips in a colloidal model of solid friction†

Erez Janai,[a] Alexander V. Butenko,[a] Andrew B. Schofield[b] and Eli Sloutskin *[a]

Received 31st March 2019,
Accepted 13th June 2019

DOI: 10.1039/c9sm00654k

rsc.li/soft-matter-journal

The intermittent 'stick-slip' dynamics in frictional sliding of solid bodies is common in everyday life and technology. This dynamics has been widely studied on a macroscopic scale, where the thermal motion can usually be neglected. However, the microscopic mechanisms behind the periodic stick-slip events are yet unclear. We employ confocal microscopy of colloidal spheres, to study the frictional dynamics at the boundary between two quasi-two-dimensional (2D) crystalline grains, with a single particle resolution. Such unprecedentedly-detailed observations of the microscopic-scale frictional solid-on-solid sliding have never been previously carried out. At this scale, the particles undergo an intense thermal motion, which masks the avalanche-like nature of the underlying frictional dynamics. We demonstrate that the underlying sliding dynamics involving out-of-plane buckling events, is intermittent and periodic, like in macroscopic friction. However, unlike in the common models of friction, the observed periodic frictional dynamics is promoted, rather than just suppressed, by the thermal noise, which maximizes the entropy of the system.

Introduction

Since the invention of fire[1] and the construction of ancient pyramids,[2] till modern-day nanorobotics,[3] frictional sliding of solid surfaces plays a pivotal role in technology. Commonly, the frictional motion is jerky, composed of (quasi-)periodic series of slip and stick events.[1] Everyday examples of such intermittent motion include the squeak of hinges, earthquakes, and the music of violins.[4] The stick-slip dynamics is reproduced by several classical theoretical frameworks, such as the Frenkel–Kontorova and the Prandtl–Tomlinson models; however, the microscopic physical mechanism responsible for the intermittent sliding in experimental systems is yet unknown. Most experimental[2,5,7] and theoretical[1,6] studies of friction completely neglect all thermal effects. Yet, thermal motion may potentially be important for nano-scale friction,[8] such as in some geological systems[9] and in grain boundary sliding, which is blamed for the 'reverse Hall-Petch' softening of nanocrystalline matter.[10] The thermal noise has been demonstrated to assist overcoming potential barriers during the frictional sliding.[11] Also, it was suggested to suppress the intermittence of particle sliding over a static periodic potential,[12] such as in the recent experimental realizations of the Frenkel–Kontorova model.[13,14] The role of thermal noise as a promoter of unsteady periodic motion has never been considered.

We study by direct confocal microscopy, grain boundary sliding of quasi-two-dimensional crystals of colloids, micron-size spheres in a solvent, where the intermittent dynamics is both promoted and masked by the thermal noise. None of the previous experimental studies of friction allowed the dynamics of individual particles, of which a solid matter is composed, to be directly visualized during frictional sliding. We demonstrate that the motion occurs through series of collective avalanche-like events, accompanied by periodic buckling of the crystal into the third dimension. Complementing our experiments by simple computer simulations, we demonstrate that the intermittent sliding dynamics is not only suppressed, but also promoted by the particles' thermal motion.

Methods and materials

Experimental system

To form the crystals, we first suspend PMMA [poly(methyl methacrylate)] spheres in dodecane (Sigma-Aldrich, $\geq$99%). The diameter of our particles is σ = 2.4 μm, as measured by scanning electron microscopy and light scattering[15] and their low polydispersity $\leq$5% facilitates crystal formation. The particles, fluorescently-labelled for confocal imaging by Nile Red dye and sterically-stabilized by a polyhydroxystearic acid monolayer (PHSA),[16] settle to the bottom of the sample container, which is a borosilicate Vitrocom™ 0.1 × 2 × 50 capillary, precoated[17] with PHSA and sealed with epoxy. Thus, a polycrystalline solid bilayer is formed at the bottom of the capillary, with the individual crystalline domains separated by high angle ($\sim$20°) grain boundaries. This sample preparation procedure ensures that a small fraction (<1%) of particles within the crystalline

[a] *Physics Department and Institute of Nanotechnology & Advanced Materials, Bar-Ilan University, Ramat-Gan 5290002, Israel. E-mail: eli.sloutskin@biu.ac.il*
[b] *The School of Physics and Astronomy, University of Edinburgh, Edinburgh EH9 3FD, UK*
† Electronic supplementary information (ESI) available: See DOI: 10.1039/c9sm00654k

domains, irreversibly stick to the bottom of the sample-containing capillary. These completely-immobilized particles partially obstruct the sliding of the crystalline domains. The random spatial distribution of these obstacles warrants that a non-zero sliding velocity mismatch would, in general, be present between the adjacent crystalline domains. To induce a drift of the bilayer we slightly tilt the capillary away from the horizontal plane, employing a tilt stage with a resolution of 0.05°, so that the component of the earth's gravity force along the crystalline plane is non-zero; thus, a controllable drift velocity v_d results. With typical experimental runs lasting for $\sim$30 min, allowing for the thermal vibration of the crystalline lattice to be averaged out, drifts smaller than 1 nm s^{-1} are readily detected. The density mismatch $\sim$0.3 g cc^{-1} between PMMA and dodecane, sets the sedimentation length of the particles to be $<0.1\sigma$; thus, the thermal motion of the particles is essentially two-dimensional.[17] To image our colloids, we employ the Nikon A1R confocal laser scanning microscope in the resonant scanning mode, at $\sim$0.17 μm pix^{-1}, close to the optical resolution. The typical field of view is 85 × 85 μm^2 and the frame rate is $\sim$4 fps. To detect all particle centers within the bottom layer of the crystalline bilayer, we employ the PLuTARC image-analysis codes, based on the modified version of the algorithm of Crocker and Grier.[18,19] The detected center positions are then fed into an iterative algorithm,[20] which minimizes the effect of finite pixel size on the accuracy of particle localization. The accuracy of this algorithm in 2D has been previously estimated[20] as $\sim$4 nm, so that very small particle displacements are accurately measured. To quantify the local crystallinity around a given particle, we employ the local six-fold-symmetric orientational bond order parameter[21] $\psi_6 = Z^{-1}\sum_i \mathrm{Re}\{\exp(6i\Delta\theta_i)\}$; here the summation is carried out over the bonds to all Z nearest neighbors (NNs) of the particle, and the angle $\Delta\theta_i$ of the i-th bond is measured in a frame oriented with one of the NN bonds, chosen at random. A particle surrounded by Z = 6 NNs in a perfectly hexagonal arrangement has ψ_6 = 1. Decreased ψ_6 values are detected at the grain boundaries. The time trajectories of the located particles are tracked by proximity:[19] particles appearing the closest together in the consecutive images, are linked, provided that their mutual separation is below 0.4σ. The tracked trajectories, which were typically $\sim$30 min-long for >1000 particles, were then carefully examined, to rule out any tracking artifacts. Finally, we de-drift the particles, by adopting the center of mass frame of the polycrystalline sample.

Molecular dynamics (MD) simulations

Molecular dynamics simulations have been carried out with LAMMPS,[22] running in the serial mode. A typical system included 40 × 20 particles. The Weeks–Chandler–Andersen (WCA) potential was adopted to account for all of the pair interactions, including the interactions between the immobilized and the free particles:

$$u(r) = \begin{cases} 4\varepsilon\left[(\tilde{\sigma}/r)^{12} - (\tilde{\sigma}/r)^{6} + c_1\right] & r < r_c \\ 0 & r \geq r_c \end{cases}, \qquad (1)$$

where c_1 = 1/4 and $r_c = 2^{1/6}\tilde{\sigma}$, with the parameter $\tilde{\sigma}$ used to define convenient MD length units. Setting k_B = 1, we fix the interaction energy parameter ε to have ε/T = 8, warranting that the system crystallizes when at equilibrium. The adopted purely-repulsive WCA potential closely approximates the almost-hard particle interactions in our experimental system;[17] yet, this potential is continuous, allowing for the numerical integration of the equations of motion. The Langevin thermostat at temperature T_{LJ} [in Lennard-Jones (LJ) units] is applied throughout, with the damping parameter and the particle mass set to 1.0 and the time step chosen as $\tau = 10^{-3}$ (LJ units). The particles are subject to a driving force F_{ext}, along the long dimension of the simulation cell (x-axis); the magnitude of this force is F_{ext} = 3 (LJ units), unless the value is explicitly specified in the text. In addition, a Hookean $(1/2)Kz^2$ potential is applied, where z is the out-of-plane coordinate. This potential, with K/T = 100 kept constant, limits the particles' out-of-plane motion to amplitudes close to the experimental ones. Initially, the particles are arranged as an hexagonal monolayer crystal, with one of its unit vectors – parallel to the x-axis. The lattice constant is 1.13σ and periodic boundary conditions are applied. One of the particles, near the middle of the y-axis range, is immobilized, partially obstructing the F_{ext}-driven flow.

Results and discussion

With the lattice constant being $\sim 1.1\sigma$, and the particle interactions – almost completely hard,[17] the dynamics of our crystals is totally dominated by thermal vibrations (see Movie 1, ESI†). This is the situation even in the lab-frame, where the center of mass is (slowly) drifting. However, tracking the particles next to a grain boundary demonstrates that the adjacent crystalline domains undergo grain boundary sliding (Fig. 1). Remarkably, while recent experimental models provide an important insight into the microscopic details of frictional sliding,[3,13] these works include only one sliding solid; the second solid is modeled by a periodic optical potential[3,13] or an AFM tip.[23] Moreover, in these works, the relevant energy scales typically far exceed k_BT, so that the thermal vibrations of the solids are totally insignificant. Similarly, thermal motion is neglected in the classical Frenkel–Kontorova

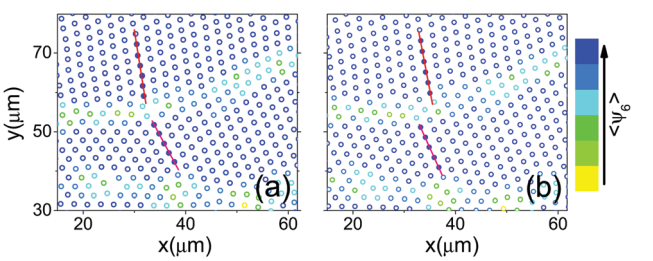

Fig. 1 Adjacent crystalline grains exhibit a grain boundary sliding. The particle center positions (circles) at time (a) t = 0 and (b) $t \approx$ 30 min are shown, with the crystals' center of mass frame adopted, to compensate for the drift. The color mapping shows the particles' local crystalline order parameter ψ_6, with the perfect crystals appearing in blue and the grain boundaries – in cyan and green. To clearly resolve the relative displacement of the two grains, we mark (the same) 11 particles in (a) and (b), by filled symbols and red lines. The full dynamics are shown in Movie 1 (ESI†).

and Prandtl–Tomlinson theoretical models.[1] Notably, in many real-life situations, significant thermal vibrations[24] must be present in frictional sliding at atomic and molecular length scales, especially near the melting point of one (or both) of the solids, where grain boundary sliding is most common. The amplitudes of particle vibrations scaled by the lattice constant a, are in fact similar in our system and in atomic crystals near melting.[25,26] Also, the tendency for thermal structural relaxation in our system is similar to that in the common frictional sliding. We quantify this tendency by the ratio between the time for a free particle to pass lattice constant distance a by thermal motion and a/v_d, where v_d is the drift velocity (with respect to the immobilized-particle obstacles). In our colloidal system, this ratio, known as the Péclet number,[15] is $0.04 < \mathrm{Pe} < 0.5$. In an atomic solid, the (ballistic) thermal velocity of atoms of mass m is $v_T \approx \sqrt{3k_BT/m}$, and the tendency for thermal relaxation may be characterized by v_d/v_T. For example, for this ratio in sliding of iron ($m \approx 9.3 \times 10^{-26}$ kg) at $v_d \approx 1$ m s^{-1} to be comparable to the Pe in our colloidal system, the temperature of iron should be $10^{-2} < T < 1$ K. Notably, for higher temperatures and smaller sliding velocities, the tendency for thermal relaxation would be even higher, emphasizing the importance of thermal lattice vibrations in everyday frictional sliding situations.

According to the second law of thermodynamics, thermal noise tends to increase disorder. Therefore, the sequence of periodic stick-slip events must be blurred when thermal lattice vibrations of the sliding solids are significant. Indeed, thermal noise was demonstrated to induce a crossover from an intermittent to a smooth sliding, in computer simulations of colloids driven over a periodic potential.[12] Remarkably, in our system, where particle interactions are closely approximated by hard repulsion potentials,[17,18] it is the entropy which makes the individual grains preserve their structural integrity.[27] As hard particle crystals owe their existence to the number of crystalline microstates at high densities exceeding the number of structurally-disordered microstates,[28] the elastic moduli of such crystals are entropic in origin.[29] In our case, the experimental time scales are far too short for the system to reach its ground state, a single crystal with no grain boundaries. However, the structural disorder is concentrated only at the grain boundaries (Fig. 1), indicating that the entropy gain due to the more efficient packing in the bulk of the grain, dominates. This entropic stabilization of grains' crystallinity sets our system apart from the classical granular models of polycrystalline matter, such as the Nye–Bragg bubble rafts, where strong interparticle attractions dictate the physical behavior.[30,31] Our mechanism of entropic stabilization can only be realized when the system is capable of exploring its phase space, at least in the local manner. In our case, the phase space is explored by the thermal motion, with the propagation of structural disorder from the grain boundary into the bulk of the crystalline grains (Fig. 1) prohibited by entropy. Thus, the thermal noise plays here a dual role, both stabilizing the sliding solids and blurring the stick-slip events.

Strikingly, while the intense thermal vibrations of the lattice mask the intermittent nature of the grain boundary sliding, this intermittency reemerges in the time-averaged particle positions. To demonstrate this intermittency, we first window-average the particle positions in time to minimize the effect of thermal noise (window size = 65 s). Then, we overlay the resulting averaged particle positions within a time window of 250 s, so that the positions of mobile particles are slightly smeared in the direction of their motion. The resulting video (Movie 2, ESI†) clearly demonstrates that the motion is unsteady: in some frames, all particles appear point-like [Fig. 2(a)], indicating that no dynamic events occur within the corresponding time period of 250 s; in other frames, many particles are mobile, as indicated by their window-averaged positions being smeared in a certain direction [Fig. 2(b)].

Remarkably, the intermittent sliding of the particles is accompanied by a similarly-intermittent buckling of the quasi-2D crystalline layer, with some of the particles pushed out of the confocal imaging plane. To quantify this effect, we count the number of particles $N(t)$ in the confocal image. As for the particle positions, we average-out the high-frequency noise of $N(t)$, employing an adjacent averaging with a window of 26 s. The resulting particle number variation about the mean $\Delta N(t)$ is shown in Fig. 3 (solid black curves); note the periodicity of these data. Notably, $\Delta N(t)$ is anticorrelated with the sliding velocity $v_s(t)$ of the grains [orange dash-dotted curve in Fig. 3(a)]: during an out-of-plane buckling event, $\Delta N(t)$ is the lowest and the sliding velocity $v_s(t)$ is the highest (see also the inset to Movie 1, ESI†). The observed anticorrelation suggests that the slip events are enabled by the out-of-plane buckling of the crystalline grains. As the stress which drives the buckling is released upon a slip event, the sliding stops, waiting for the buildup of a sufficient stress for the next buckling event to occur. The intermittent motion of the grain boundary, changing its shape abruptly, in-phase with the stick-slip events, is clearly observed in Movie 3 (ESI†), where particles are color-mapped by their coordination number Z. The same is shown in Movie 4 (ESI†), where all particles for which $Z = 6$ appear transparent, to emphasize the location of the grain boundary.

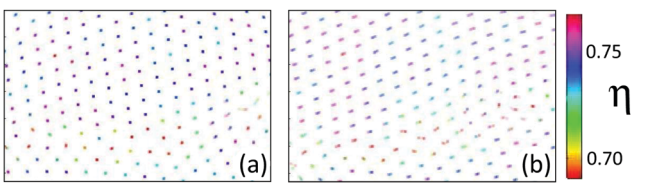

Fig. 2 The particle positions, with the time scales corresponding to thermal vibrations averaged-out, exhibit a non-steady drift. The intermittent nature of this drift is demonstrated by overlaying these averaged particle positions within a time window of 250 s. Particle positions are point-like in section (a), indicative of a 'stick'-like event, where particles undergo thermal vibrations, yet no net sliding takes place (except for a few particles on the right side of the image). A 'slip' event is observed in (b), where particle positions are smeared. The particles are color mapped according to their local area fraction $\eta = A_0/A_V$, where $A_0 = \pi\sigma^2/4$ and A_V is the area corresponding to a given particle in the Voronoi tessellation.[32] Note the larger fluctuations in η at the grain boundaries, with η occasionally exceeding its average bulk value due to the out-of-plane protrusion by some of the particles;[21] with the present color map, these fluctuations make the grain boundaries appear slightly more reddish, compared to the bulk of the crystals. See the full dynamics presented in Movie 2 (ESI†).

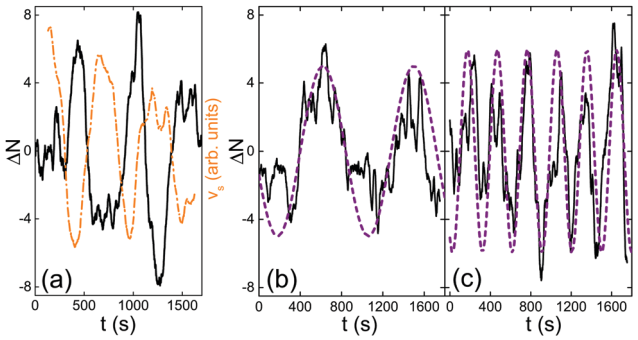

Fig. 3 The buckling of particles out of the plane exhibits a clear periodicity, as demonstrated by the oscillations of the particles' number within the crystals $\Delta N(t)$ (solid black curves), for drift velocities: (a) v_d = 4.9 nm s^{-1}; (b) v_d = 2.5 nm s^{-1}; (c) v_d = 8.4 nm s^{-1}. During a buckling event [a minimum of $\Delta N(t)$], the grain boundary sliding is on, as indicated by a maximum in the grain sliding velocity $v_s(t)$ (orange dash-dotted curve in (a)). The experimental data in (b) and (c) are fitted by a sine function (purple dashes), allowing the frequency of oscillations to be extracted [see Fig. 4]. Note the very good match with the experiment.

The periodic nature of $\Delta N(t)$ allows its frequency of oscillations f to be extracted by fitting to it a simple sine function. Note the very good match between the fit (purple dashes) and the experiment (solid black curves) in Fig. 3(b and c). Interestingly, the frequency of these oscillations increases with v_d, the drift velocity through the suspending medium [*cf.* Fig. 3(a–c)]. Repeating the same experiment for a wide range of v_d values, we obtain a linear $f(v_d)$ dependence, demonstrated in Fig. 4. Remarkably, the data do not show any systematic behavior when plotted as a function of the relative sliding velocity of the individual grains, excluding the intra-grain interactions as a possible cause of the intermittent slip-stick motion. The linear dependence of f on the absolute drift velocity suggests that the buckling (and consequently, the sliding) events are controlled by the crystals' interaction with static obstacles, particularly the particles which are immobilized at the capillary wall. Indeed, the average displacement of the crystalline grain between two successive buckling events, $v_d/f \approx 2.8$ μm, almost perfectly matches the lattice constant of our crystals, $a \approx 2.6$ μm. Thus, the buckling (and the consequent sliding) events take place whenever the position of an immobilized particle is incommensurate with the lattice, a situation occurring every ∼2.6 μm of the sliding.

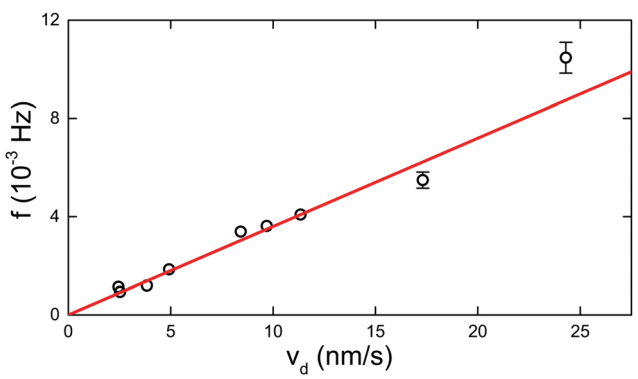

Fig. 4 The frequency of $\Delta N(t)$ variations is proportional to the drift velocity v_d of the grains through the suspending medium, vanishing for v_d = 0. A linear fit is shown in red.

Computer simulations

The identification of a relatively simple mechanism as being responsible for the intermittent motion in our system, allows a further insight into its physics to be gained by molecular dynamics simulations. Employing Langevin dynamics, we simulate a monolayer crystal of short-range-repulsive (almost hard) colloids, driven by a time-independent external force through a viscous fluid (see Methods). One of these colloids is immobilized, posing an obstacle for the motion of the crystal. Exactly as in our experiments, the interaction between the static obstacle and the driven crystal gives rise to an intermittent motion of the crystal (see Movie 5, ESI†). While, as in the experiments, the intermittent nature of the simulated crystal's sliding is masked by the thermal noise, averaging the center of mass (CM) positions of the crystal over 50 time steps uncovers the periodicity of this motion [see orange squares in Fig. 5(a)]. Moreover, the slip events are associated with the

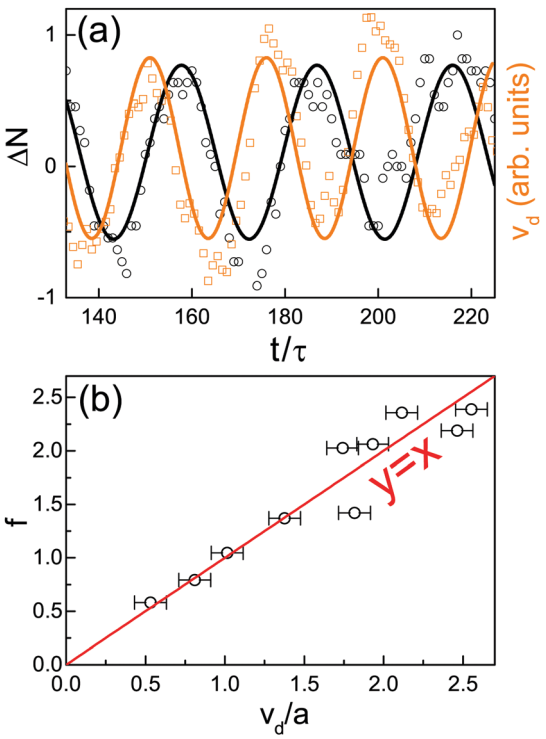

Fig. 5 (a) The simulated velocity v_d of the center-of-mass (CM) of the crystal, with the thermal noise averaged-out (see text), is intermittent and periodic (orange scatter). The out-of-plane buckling of the particles, quantified by ΔN is periodic as well. As in the experiments [Fig. 3(a)], v_d and ΔN exhibit opposite phases, supporting our simulations. Here ΔN is the fluctuation in the number of particles located at $|z| > 0.1$, within the radius of 2 LJ units from the immobilized obstacle; the thermal noise is averaged-out, as in the experiments. The ΔN amplitude depends on the number of immobilized particles within the region of interest, which is smaller in the simulations. Both data sets are fitted by sine functions (solid curves). F_{ext} = 2.7. (b) The simulated frequency of the slipping events (circles) is equal to the average velocity of the crystal v_d, normalized by the lattice constant a. The red diagonal line ($y = x$) perfectly matches the simulated data, demonstrating that these simple simulations fully match our experiments. T_{LJ} = 70 in both (a) and (b).

out-of-plane buckling events, as demonstrated by the phase of ΔN oscillations being opposite to that of v_d [Fig. 5(a)]: the stress due to the interaction with the immobilized particle, makes the crystal periodically buckle into the third dimension, which in turn allows the slip events to take place. As detailed above, a similar behavior takes place in our experiments [*cf.* Fig. 3(a) and 5(a)], strongly supporting the validity of our simplified simulations.

To further support our simulations, we also tune the time-averaged sliding velocity v_d by varying the external driving force. The frequency of the slip events scales linearly with v_d. Moreover, $f \approx v_d/a$, demonstrating that in these simulations, like in the experiments, the buckling events occur when the position of the immobilized particle is incommensurate with the crystalline lattice (*cf.* Fig. 4 and 5(b)). Thus, these simulations correctly reproduce our main experimental observations.

Having established a match between the simulations and the experiments, we now employ the simulations to explore the dependence of the slip-stick motion on temperature, testing for the role of entropy in these phenomena. Importantly, this dependence cannot be studied with our experimental system, as the stability of the colloidal suspension may be disrupted by significantly changing its absolute temperature away from the ambient $T = 297$ K. Remarkably, the average sliding velocity of the crystal, for a given driving force F_{ext}, reduces with T [Fig. 6(a)]. This, somewhat counter-intuitive, increase in crystal hardness on heating is explained by the crystal-promoting role played here by the entropy. The role of entropy as a stabilizer of crystals is very well known for particles interacting through an ideally-hard potential, where the energy scale is completely missing.[29] In dense systems of such particles, each particle gains an additional free volume (and consequently more entropy) when the particles form a crystalline structure. Moreover, the stiffness of such a structure increases with the temperature, contrasting with the behavior of energy-stabilized crystals, such as the ionic crystals,[11] which typically soften at high T. Our particles, both the experimental and the simulated ones, are sufficiently close to the hard particle limit, so that the entropy's role as a promoter of crystallinity is still retained, even though the interactions are not perfectly hard.

As typical for the entropic effects, the slip-stick motion disappears at a lower temperature, where the steady motion is reestablished [inset to Fig. 6(b)]. With the particles' diffusion being slower at low T, the particles are unable to explore their local phase space, so that the structure in the immediate vicinity of the obstacle, fluidizes [see Movie 6 (ESI†) and inset to Fig. 6(a)]. To quantitatively characterize the T-controlled transition between the intermittent motion and the continuous sliding, we first fit the CM position of the crystal (with the thermal noise averaged-out as above) by a monotonic function. The residual sum of squares χ^2, measures the extent of the intermittent behavior. Remarkably, χ^2 strongly increases with T [Fig. 6(b)], confirming the entropic origin of the observed stick-slip dynamics. Finally, we expect a similar behavior to take place in smooth metallic monolayers, where the interactions are similarly dominated by hard repulsions.[33,34] However, the onset of the entropy-driven stick-slip dynamics is expected to occur at an ultra-low T, where $v_T/v_d \approx 1$.

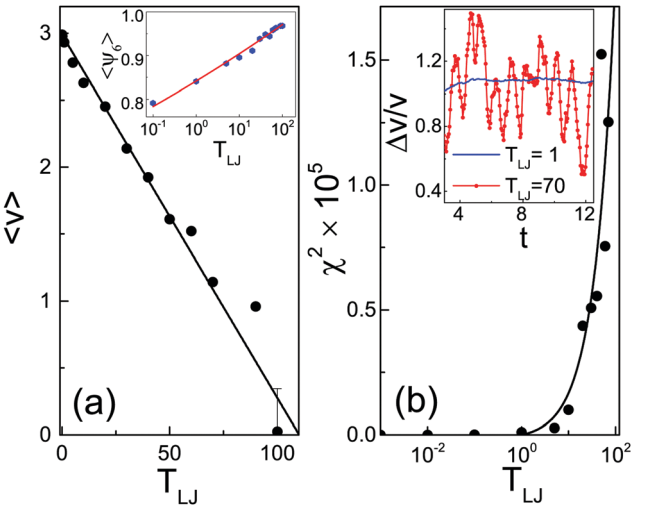

Fig. 6 Entropy-promoted periodic slip-stick motion of a simulated colloidal crystal, driven by a constant external force and slowed-down by its interaction with a static obstacle. The velocity of the center-of-mass (CM) of the crystal, with the thermal noise averaged-out (see text), is strongly oscillating at high T [connected red symbols in the inset to (b)]. At lower T, the motion is much smoother [blue line in the inset to b] and the average velocity is faster [see (a)]. Moreover, a local melting of the sample is induced by the static obstacle at low T_{LJ}, as evidenced by the reduced values of the sample-averaged two-dimensional crystalline order parameter $\langle\psi_6\rangle$ [inset to (a)]. Note the onset of the intermittent slip-stick dynamics, which is manifested by the dramatic increase of χ^2 at $T_{LJ} > 1$, in (b); here χ^2 measures the deviations from the perfectly-monotonic motion of the CM (see text). Importantly, the enhancement of the slip-stick oscillations' amplitude with T is a strong evidence confirming that the origin of these oscillations is entropic. All quantities are expressed in LJ units (see Methods). See the behavior at $T_{LJ} = 1$ and at $T_{LJ} = 90$, in Movies 6 and 5 (ESI†), respectively.

Conclusions

We have established an experimental colloidal model, allowing the grain boundary sliding to be visualized by direct optical microscopy, with a single particle resolution. In this model, as in the conventional atomic solids, significant thermal vibration of the lattice takes place. With the particles exploring their local phase space at rates much faster than the sliding, the crystallinity of the grains is maintained by the entropy, so that the disorder is localized at the grain boundaries and stick-slip frictional dynamics emerges. We have demonstrated that the stick-slip dynamics of these entropically-stabilized solids is periodic, with slip onsets coinciding with the out-of-plane buckling events. Future studies should allow the strain and the stress fields within each of the solids undergoing friction to be analyzed, for a wide range of particle interaction potentials. Highly-detailed experimental information thus achieved, should potentially allow a full understanding of the physical mechanisms of solid-on-solid atom-scale frictional dynamics to be established.

Additional information on the ESI movies†

Movie 1

The tracked particle center positions, obtained by confocal microscopy, are shown as solid dots. Note the very strong thermal

vibration of the particles, dominating their motion. Two groups of particles, belonging to different crystalline grains, are marked in red, allowing the relative sliding of the two grains to be visualized. The deviation of the particles' number from the average ΔN, due to the out-of-plane buckling (see main text and Fig. 3(a)), is shown in the inset, as a function of time.

Movie 2

Particle positions (with the thermal vibrations averaged-out) are overlayed within a window of 250 s, demonstrating the intermittent stick-slip dynamics. In an absence of slip, the overlayed particle positions overlap, so that the particles appear point-like; smeared particle positions correspond to the slip events. A few representative particles are marked by a red circle, surrounding them when they are immobilized, between the slip events. All the particles are color-mapped by their local area fraction η (see main text), strongly fluctuating at the grain boundary; with the present choice of the color map, the η fluctuations make the grain boundaries appear slightly more reddish, compared to the bulk of the crystals. The movie corresponds to 0.5 h of real time.

Movie 3

The same as Movie 2, but with the particles color-mapped by their coordination number. The nearest-neighbors are detected by the Delaunay triangulation algorithm. Note the formation and the annihilation of paired five- and seven-fold defects, associated with the out-of-plane buckling of individual particles.

Movie 4

The intermittent motion of the grain boundary is emphasized by showing (for the same data as in Movie 3) only those particles, which have their coordination number different from 6. Note the periodic displacements of the grain boundary, corresponding to grain boundary slipping events.

Movie 5

Computer simulations of a crystal, which has its drift partially obstructed by an immobilized particle. Note that the motion is intermittent. The build-up of the elastic stress makes one of the particles in the vicinity of the static obstacle to be pushed out of the crystal plane. Then, a slip event takes place, relieving the stress and allowing the particle to return back to the crystal plane. The out-of-plane height (z) of the particles is encoded by their color. Particles within the crystal plane ($z = 0$) are blue. Here $T_{LJ} = 90$ (see Fig. 6 and Methods).

Movie 6

The same as in Movie 5, but at $T_{LJ} = 1$. Note that the drift is now smooth, with the immediate vicinity of the obstacle – fluidized. With the temperature being lower than in Movie 5, the particles are unable to explore their local phase space, so that the effective rigidity of the crystal is reduced and the intermittent slip-stick motion is absent.

Conflicts of interest

There are no conflicts to declare.

Acknowledgements

We are grateful to Peter J. Lu for sharing his PLuTARC codes, to Dov Fridman for technical assistance, and to Erio Tosatti for illuminating discussions. This research was supported by the Israel Science Foundation (grant no. 1779/17). Some of the equipment was funded by the Kahn foundation. ABS is partially funded by the UK Engineering and Physical Sciences Research Council grant EP/J007404/1. The paper is dedicated to Prof. Peter Pershan (Harvard University) a trail blazer in Surface Science, on his 85th birthday.

References

1 M. H. Müser, M. Urbakh and M. O. Robbins, *Adv. Chem. Phys.*, 2003, **126**, 187–272.
2 A. Fall, B. Weber, M. Pakpour, N. Shahidzadeh, J. Fiscina, C. Wagner and D. Bonn, *Phys. Rev. Lett.*, 2014, **112**, 175502.
3 A. Bylinskii, D. Gangloff and V. Vuletić, *Science*, 2015, **348**, 1115–1118.
4 T. Palberg and K. Streicher, *Nature*, 1994, **367**, 51–54.
5 S. M. Rubinstein, G. Cohen and J. Fineberg, *Nature*, 2004, **430**, 1005–1009.
6 M. Nosonovsky, *J. Chem. Phys.*, 2007, **126**, 224701.
7 A. D. Berman, W. A. Ducker and J. Israelachvili, *Langmuir*, 1996, **12**, 4559–4563.
8 M. Reguzzoni, M. Ferrario, S. Zapperi and M. C. Righi, *Proc. Natl. Acad. Sci. U. S. A.*, 2010, **107**, 1311–1316.
9 S. Siman-Tov, E. Aharonov, A. Sagy and S. Emmanuel, *Geology*, 2013, **41**, 703–706.
10 J. Schiøtz, F. D. Di Tolla and K. W. Jacobsen, *Nature*, 1998, **391**, 561–563.
11 E. Gnecco, R. Bennewitz, T. Gyalog, Ch. Loppacher, M. Bammerlin, E. Meyer and H.-J. Güntherodt, *Phys. Rev. Lett.*, 2000, **84**, 1172–1175.
12 J. Hasnain, S. Jungblut and C. Dellago, *Soft Matter*, 2013, **9**, 5867–5873.
13 T. Bohlein, J. Mikhael and C. Bechinger, *Nat. Mater.*, 2012, **11**, 126–130.
14 A. Vanossi, N. Manini and E. Tosatti, *Proc. Natl. Acad. Sci. U. S. A.*, 2012, **109**, 16426–16433.
15 S. R. Liber, S. Borohovich, A. V. Butenko, A. B. Schofield and E. Sloutskin, *Proc. Natl. Acad. Sci. U. S. A.*, 2013, **110**, 5769–5773.
16 U. Gasser, E. R. Weeks, A. B. Schofield, P. N. Pusey and D. A. Weitz, *Science*, 2001, **292**, 258–262.
17 E. Janai, A. P. Cohen, A. V. Butenko, A. B. Schofield, M. Schultz and E. Sloutskin, *Sci. Rep.*, 2016, **6**, 28578.
18 P. J. Lu, M. Shutman, E. Sloutskin and A. V. Butenko, *Opt. Express*, 2013, **21**, 30755–30763.
19 J. C. Crocker and D. G. Grier, *J. Colloid Interface Sci.*, 1996, **179**, 298–310.
20 Y. Gao and M. L. Kilfoil, *Opt. Express*, 2009, **17**, 4685–4704.

21 E. Janai, A. V. Butenko, A. B. Schofield and E. Sloutskin, *J. Phys. Chem. C*, 2016, **120**, 8392–8398.
22 S. Plimpton, *J. Comput. Phys.*, 1995, **117**, 1–19.
23 R. Pawlak, W. Ouyang, A. E. Filippov, L. Kalikhman-Razvozov, S. Kawai, T. Glatzel, E. Gnecco, A. Baratoff, Q. Zheng, O. Hod, M. Urbakh and E. Meyer, *ACS Nano*, 2016, **10**, 713–722.
24 L. Jansen, H. Hölscher, H. Fuchs and A. Schirmeisen, *Phys. Rev. Lett.*, 2010, **104**, 256101.
25 Z. Wang, F. Wang, Y. Peng and Y. Han, *Nat. Commun.*, 2015, **6**, 6942.
26 P. Schall, I. Cohen, D. A. Weitz and F. Spaepen, *Nature*, 2006, **440**, 319–323.
27 P. Tan, N. Xu and L. Xu, *Nat. Phys.*, 2014, **10**, 73–79.
28 J.-P. Hansen and I. R. McDonald, *Theory of simple liquids*, Elsevier, USA, 2006.
29 Z. Cheng, J. Zhu, W. B. Russel and P. M. Chaikin, *Phys. Rev. Lett.*, 2000, **85**, 1460–1463.
30 L. Bragg and J. F. Nye, *Proc. R. Soc. A*, 1947, **190**, 474–481.
31 P. Singh, D. D. Joseph, S. K. Gurupatham, B. Dalal and S. Nudurupati, *Proc. Natl. Acad. Sci. U. S. A.*, 2009, **106**, 19761–19764.
32 B. A. Schultz, P. F. Damasceno, M. Engel and S. C. Glotzer, *ACS Nano*, 2015, **9**, 2336–2344.
33 B. B. Laird, *J. Chem. Phys.*, 2001, **115**, 2887–2888.
34 P. Ascarelli and R. J. Harrison, *Phys. Rev. Lett.*, 1969, **22**, 385–388.